PATTERN FORMATION IN VERTICALLY VIBRATED GRANULAR LAYERS: EXPERIMENT AND SIMULATION

M. D. SHATTUCK, C. BIZON, PAUL B. UMBANHOWAR, J. B. SWIFT AND
HARRY L. SWINNEY
Center for Nonlinear Dynamics
and Department of Physics
The University of Texas at Austin
Austin, TX 78712

Abstract.

   We report on pattern formation in experiments and simulations of vertically vibrated granular layers. We find that initially flat vibrated layers lose stability to sub-harmonic standing wave patterns when the driving acceleration is increased to about 2.5 times gravity. Patterns can be squares, stripes, hexagons, or localized structures (*oscillons*), depending on frequency and acceleration. Event driven simulations show excellent qualitative and quantitative agreement with the experiments.

1. Introduction

In this article, we review our recent work on pattern formation in vertically vibrated granular layers [1, 6, 7, 11]. Other similar experiments showing convection and heap formation [2], size segregation [3], and bubbling [8] result from a combination of side wall friction and interaction with the interstitial gas [9]. In our experiments we diminish these effects by using thin layers (i.e., the horizontal size of the system is much larger than the depth), which limits the effects of the walls, and evacuating the system, which eliminates the interaction with interstitial gas. Under these conditions vertically vibrated granular layers yield a variety of standing wave patterns which oscillate at either one-half or one-quarter of the vibration frequency f. The planform of the pattern is determined by two control parameters, f and the acceleration amplitude, $\Gamma = 2\pi A f^2 / g$, where g is the gravitational acceleration constant and A is the oscillation amplitude. Depending on the values

(a)   (b)
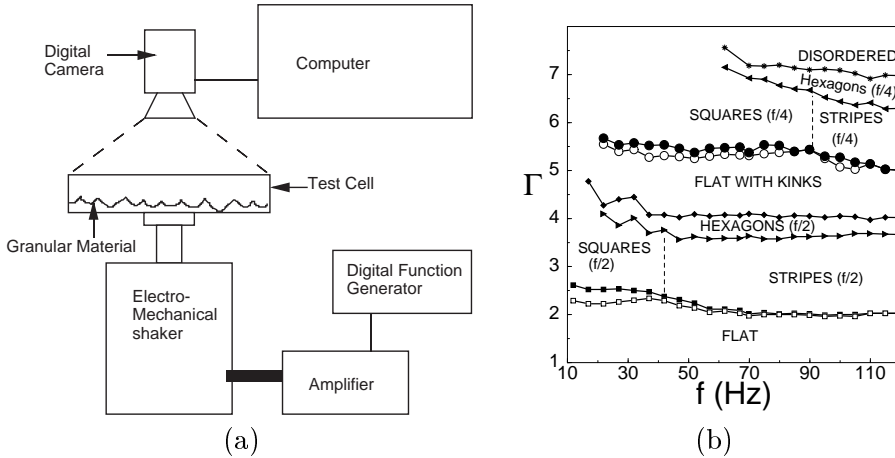
Figure 1. (a) Schematic of the experimental apparatus showing the test cell, the shaker and the imaging system. The camera can be placed above, to produce images like those in Figure 2, or to the side of the test cell, to produce images like those in the top of Figure 3(b). (b) Phase diagram for a 1.2 mm deep layer of 0.15–0.18 mm bronze spheres showing transitions between pattern states. The dashed lines indicate the square/stripe transition. Solid (open) circles and squares denote transitions with increasing (decreasing) Γ.

of Γ and f, squares, stripes, hexagons, and localized structures can be seen [6, 7, 11]. In order to facilitate a microscopic understanding of the system, Bizon et al. have developed an event driven simulation which reproduces the observations at the experimental values of the control parameters [1].

2. Experimental Apparatus

The experiment consists of a container (typically cylindrical, of diameter= 126 mm) filled with a thin layer of particles (2–30 particle diameters deep) and vibrated sinusoidally ($A\sin(2\pi ft)$) in the vertical direction by an industrial electro-mechanical shaker (see Figure 1(a)). The top and sides of the cell are transparent for visualization by a high speed digital camera; the bottom is aluminum. Many different types of particles (e.g., bronze, lead, glass, plastic, rice, etc.) and diameters (0.05–3 mm) have been used, but typically bronze spheres sieved to a range of 0.15–0.18 mm diameter are used. The physical control parameters are the amplitude A, varied up to 1 cm, and the frequency f, varied from 10 to 200 Hz. Experiments are typically performed at constant Γ and f is varied.

3. Patterns

When the layer is shaken at an acceleration below $\Gamma = 1$, it remains stationary in the reference frame of the cell. For $\Gamma_c > \Gamma > 1$, the layer separates

<center>(a)   (b)   (c)</center>
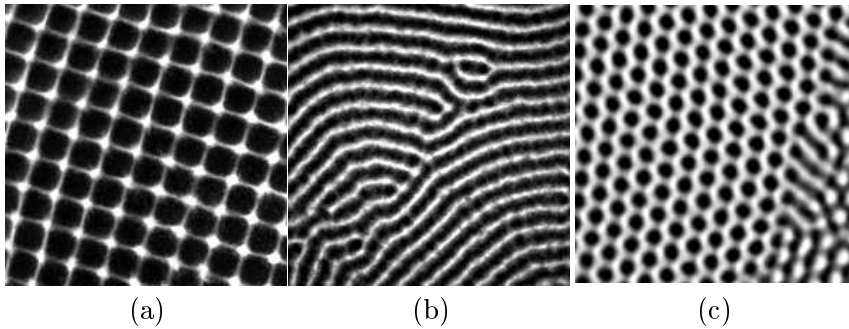
Figure 2.   Patterns formed in 0.15–0.18 mm bronze spheres in a 126 mm container. An 80 mm x 80 mm section is shown. The images are created by low angle strobed light. (a) squares, $f = 22$ Hz, $\Gamma = 2.5$, $H = 4$ particle diameters; (b) stripes, $f = 47$ Hz, $\Gamma = 2.5$, $H = 4$ particle diameters; (c) hexagons, $f = 67$ Hz, $\Gamma = 4.0$, $H = 7$ particle diameters.

from the bottom plate of the cell for a portion of the cycle, but the top and bottom surfaces of the layer remain flat, even though the layer is in free flight, until a critical acceleration Γ_c is reached and the flat layer becomes unstable to spatially periodic standing waves, which oscillate at $f/2$ [6]. As the acceleration is increased further, a bifurcation sequence is observed (Figure 1(b)). The pattern at onset has a 10% hysteresis in Γ at low frequencies and is squares at low frequencies (Figure 2(a)) and stripes (Figure 2(b)) at high frequencies. When Γ is increased to about 4, both squares and stripes lose stability to hexagons (Figure 2(c)). At still larger Γ the layer is thrown so high that it impacts the plate only once every other oscillation and hexagons become unstable to a flat layer which oscillates at $f/2$. Because the layer oscillates at $f/2$, two phases with respect to the driving frequency can co-exist in the cell forming a kink between the regions of different phase. Further increases in Γ cause the sequence of bifurcations to be repeated, except the pattern now oscillates at $f/4$. From $\Gamma = 7$ to 10 (the largest Γ studied) a disordered state exists. Melo et al. [7] explain most of this phase diagram using a simple model which treats the layer as a single totally inelastic ball.

4. Localized Structures — *oscillons*

Umbanhowar et al. [11] found that in deeper layers (> 13 particle diameters), localized structures (Figure 3) form as Γ is lowered below the point where squares or stripes are stable. The range of stability for these structures, named oscillons, is small: $2.4 < \Gamma < 2.5$ and $20 < f < 35$ Hz for a layer of 0.15–0.18 mm bronze spheres at a depth of 17 particle diameters. Oscillons are stable localized structures oscillating at $f/2$, just like the standing wave patterns described above. Figure 3(a) shows two oscillons in

(a)   (b)
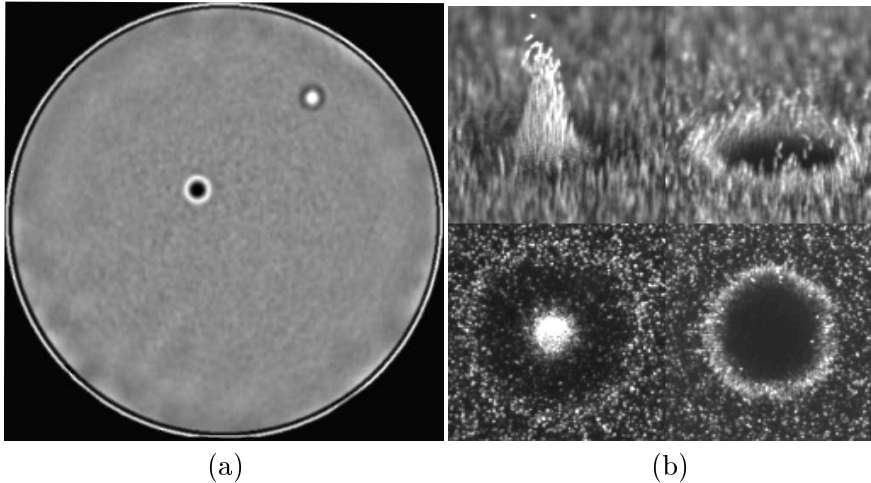
Figure 3.   (a) Oscillons observed using 0.15–0.18 mm bronze spheres, 17 particle diameters deep in a 126 mm cell at $f = 26$ Hz and $\Gamma = 2.54$. (b) Side and top views of single oscillons. The left and right images are separated by one container oscillation.

a 126 mm diameter cell. This snapshot shows that, due to the sub-harmonic nature of this pattern, two phases of oscillons can coexist. Figure 3(b) shows close up side and top views of the oscillon in each phase. Oscillons of unlike phase can bind to form pairs, chains, and other complex structures with coordination number up to three [11].

5. Numerical Simulation

In an effort to understand the pattern formation described above, and its connection to the microscopic grain interactions, Bizon et al. [1] have developed an event driven numerical simulation of this granular system [5, 4, 10]. In this type of simulation time advances from collision to collision with ballistic motion between collisions. A sorted list of the time-to-next-collision is maintained for each particle and is used to determine the next collision. The simulation advances through the collision using a model which maps the velocities and angular velocities of each particle before the collision to their values after the collision. Linear and angular momentum are conserved in collisions, but not energy. The collision duration is assumed zero, therefore limiting the particle interactions to binary collisions. Interactions with the four walls and the bottom plate are treated like particle-particle interactions with one particle's (i.e., the wall's) mass going to infinity. To test the validity of the model, experiments were conducted for conditions as close as possible to the simulation. Either 60000 or 30000 particles were used in a square container which is 100 particle diameters on each side, correspond-

(a)   (b)   (c)   (d)
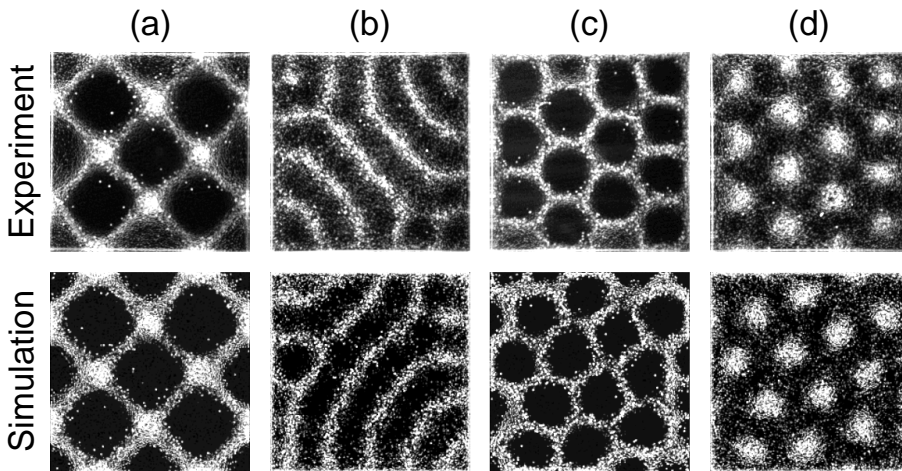
Figure 4. Comparison of standing wave patterns obtained in experiment and simulation: (a) squares, (b) stripes, (c) and (d) alternating phases of hexagons. All Patterns oscillate at f/2. The layer depth is 5.42 particle diameters. The experiments use lead spheres sieved between 0.5–0.6 mm in a container which is 100 particle diameters on each side.

ing to layer depths of $H = 5.42$ and $H = 2.71$ particle diameters respectively. Experiments and simulation are compared using a non-dimensional frequency $f^* = f\sqrt{H/g}$. In the experiment the particles were lead spheres sieved between 500 and 600 mm. In the simulation, three collisional particle properties — the coefficient of friction μ, the normal coefficient of restitution e, and the cutoff for the rotation coefficient of restitution β_0 — must be determined. The value of β_0 is taken from the literature [12, and references therein]. e and μ are determined by adjusting their values until the wavelength of the pattern in the simulation and experiment matched in two specific runs, $\Gamma = 3.0$, $f^* = 0.205$, $H = 2.71$ (for e), and $\Gamma = 3.0$, $f^* = 0.534$, $H = 5.42$ (for μ). Figure 4 shows patterns obtained in the simulation and experiment at the same values of control parameters which are denoted by points on the phase diagram (Figure 5(a)) labeled (a)–(d). The labels (e)–(h) in Figure 5(a) denote further runs which show the same excellent agreement as in Figure 4. The measured pattern wavelengths for various f^*, in experiment and simulation agree well, even when comparing the simulation in a cell 100 particle diameters wide with experiments in a large container with a diameter of 982 particle diameters (Figure 5(b)).
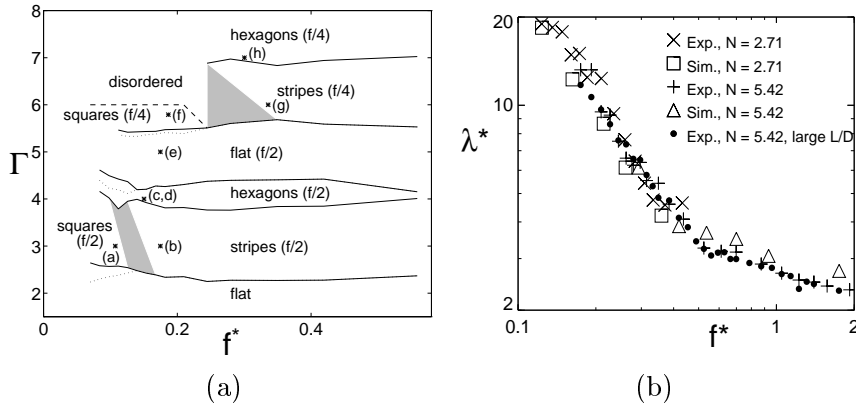
6. Acknowledgements

6

(a) (b)

Figure 5.   (a) Phase diagram from the experiments for layer depth of 5.71 particles. The parameter values used for the patterns in Figure 4 are indicated by (a) through (d). Solid lines denote the transitions with increasing Γ, and dotted lines denote transitions for decreasing Γ. Shaded areas show transitional regions between stripes and squares. (b) Wavelength vs. frequency from simulations and experiments with Γ = 3.0. The + and × points are obtained from experiments with lead spheres ($D = 0.55$ mm) in a container 100 particles on each side, while the ● points correspond to experiments with bronze spheres ($D = 0.165$ mm) in a container with a diameter 982 particles.

References

1.   Bizon, C., Shattuck, M. D., Swift, J. B., McCormick, W. D., and Swinney, H. L. (1998). Patterns in 3D vertically oscillated granular layers: Simulation and experiment. *Phys. Rev. Lett.* to to be published.

2.   Evesque, P. and Rajchenbach, J. (1989). Instability in a sand heap. *Phys. Rev. Lett.*, 62:44–46.

3.   Knight, J. B., Jaeger, H. M., and Nagel, S. R. (1993). Vibration-induced size separation in granular media: The convection connection. *Phys. Rev. Lett.*, 70(24):3728–3731.

4.   Luding, S., Clément, E., Blumen, A., Rajchenbach, J., and Duran, J. (1994). Anomalous energy dissipation in molecular-dynamics simulations of grains: The "detachment effect". *Phys. Rev. E*, 50(5):4113–4120.

5.   Marín, M., Risso, D., and Cordero, P. (1993). Efficient algorithms for many-body hard particle molecular dynamics. *J. Comput. Phys.*, 109:306–317.

6.   Melo, F., Umbanhowar, P., and Swinney, H. L. (1994). Transition to parametric wave patterns in a vertically oscillated granular layer. *Phys. Rev. Lett.*, 72:172–175.

7.   Melo, F., Umbanhowar, P. B., and Swinney, H. L. (1995). Hexagons, kinks, and disorder in oscillated granular layers. *Phys. Rev. Lett.*, 75(21):3838–3841.

8.   Pak, H. K. and Behringer, R. P. (1994). Bubbling in vertically vibrated granular materials. *Nature*, 371:231–233.

9.   Pak, H. K., Van Doorn, E., and Behringer, R. P. (1995). Effects of gases on granular materials under vertical vibration. *Phys. Rev. Lett.*, 74:4643–4646.

10.   Rapaport, D. C. (1980). The event scheduling problem in molecular dynamics simulation. *J. Comput. Phys.*, 34:184–201.

11.   Umbanhowar, P., Melo, F., and Swinney, H. L. (1996). Localized excitations in a vertically vibrated granular layer. *Nature*, 382:793–796.

12.   Walton, O. R. (1993). Numerical simulation of inelastic, frictional particle-particle interactions. In Roco, M. C., editor, *Particulate Two-Phase Flow*, pages 884–911. Butterworth-Heinemann, Boston.